

Article

In Situ Formation of TiB₂/Al₂O₃-Reinforced Fe₃Al by Combustion Synthesis with Thermite Reduction

Chun-Liang Yeh * and Chih-Yao Ke

Department of Aerospace and Systems Engineering, Feng Chia University, Taichung 40724, Taiwan; m0607494@fcu.edu.tw

* Correspondence: clyeh@fcu.edu.tw; Tel.: +886-4-2451-7250 (ext. 3963)

Received: 7 April 2018; Accepted: 19 April 2018; Published: 22 April 2018



Abstract: Fabrication of Fe₃Al–TiB₂–Al₂O₃ composites with a broad range of phase compositions was studied by combustion synthesis involving aluminothermic reduction of oxide precursors. Two reaction systems composed of elemental Fe, amorphous boron, and a thermite mixture of Fe₂O₃/TiO₂/Al were conducted in the mode of self-propagating high-temperature synthesis (SHS). One was to produce the composites of 1.25Fe₃Al + xTiB₂ + Al₂O₃ with x = 0.3–1.0. The other was to fabricate the products of yFe₃Al + 0.6TiB₂ + Al₂O₃ with y = 1.0–1.6. Reduction of Fe₂O₃ by Al acted as an initiation step to activate the SHS process. Complete phase conversion from the reactants to Fe₃Al–TiB₂–Al₂O₃ composites was achieved. The variation of combustion front velocity with sample stoichiometry was consistent with that of the reaction exothermicity. Based on combustion wave kinetics, the activation energy of E_a = 86.8 kJ/mol was determined for formation of the Fe₃Al–TiB₂–Al₂O₃ composite through the thermite-based SHS reaction. In addition, with an increase in TiB₂, the fracture toughness of the 1.25Fe₃Al + xTiB₂ + Al₂O₃ composite was found to increase from 5.32 to 7.92 MPa·m^{1/2}.

Keywords: self-propagating high-temperature synthesis (SHS); iron aluminides; Fe₃Al–TiB₂–Al₂O₃ composites; aluminothermic reduction; activation energy

1. Introduction

The iron aluminides Fe₃Al and FeAl have been of significant importance for high-temperature structural and coating applications due to their low cost, low density, relatively high melting point, high electrical resistivity, and good oxidation, corrosion, and sulfidation resistance. However, they exhibit low ductility and brittle fracture at ambient temperatures [1–3]. Efforts to strengthen iron aluminides showed that the room-temperature strength and wear resistance of Fe₃Al were greatly improved by incorporating hard carbide or boride particles (such as TiC, WC, TiB₂, and ZrB₂) [4–7]. Also, oxide ceramics are effective in reinforcing iron aluminides. The addition of Al₂O₃ and ZrO₂ particles can enhance the high-temperature strength of Fe₃Al without compromising its oxidation resistance [8–11].

A variety of processing techniques have been employed to fabricate iron aluminide–ceramic composites, including liquid-phase sintering [4], hot pressing [8,9], mechanochemical synthesis [10], solid-state displacement reactions [11], and combustion synthesis in the modes of self-propagating high-temperature synthesis (SHS) [12] and thermal explosion [13]. Among them, the SHS method takes advantage of highly exothermic reactions, and hence has the merits of a low energy requirement, a short reaction time, inexpensive equipment, simplicity of operation, and a structural and functional diversity of final products [14–16]. When combined with a thermite reaction using Al as the reducing agent, combustion synthesis represents an in situ fabrication route to prepare Al₂O₃-reinforced intermetallics

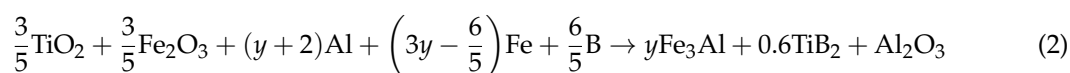
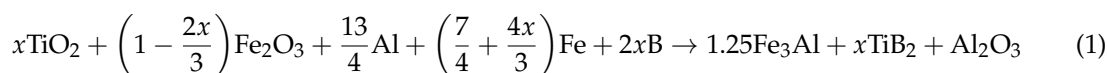
and ceramics [12,13,17,18]. Moreover, aluminothermic reduction of metal oxides is thermally beneficial for the SHS process.

Preparation of transition-metal aluminides of the Ni–Al and Ti–Al systems has been studied by the classical SHS method using elemental powder compacts of their corresponding stoichiometries [19–21]. However, direct combustion between Fe and Al powders in a compressed form to produce Fe₃Al and FeAl is not feasible because of their low formation enthalpies or high activation energy barrier. As a result, few related studies on combustion synthesis of iron aluminides are available. According to Sharifitabar et al. [12], TiC/Al₂O₃-added Fe₃Al was produced by combustion synthesis in the SHS mode from a 3TiO₂ + 4Al + 3C exothermic mixture with an addition of Fe. Liu et al. [13] obtained FeAl/Al₂O₃ composites from a reactant mixture made up of Fe, Al, and Fe₂O₃ by thermal explosion of combustion synthesis. The ignition temperatures were between 639 and 648 °C and the products were highly porous [13].

This study aims to investigate in situ formation of TiB₂/Al₂O₃-reinforced Fe₃Al composites by the SHS method involving aluminothermic reduction of Fe₂O₃ and TiO₂. In addition to the thermite reagents, the starting materials included elemental iron and amorphous boron powders. Effects of TiB₂ and Fe₃Al contents on combustion characteristics were studied. The activation energy of the Fe₂O₃–TiO₂–Al–Fe–B combustion system was deduced from the measured combustion wave velocity and temperature. Moreover, the strengthening effect of TiB₂/Al₂O₃ on Fe₃Al was examined.

2. Materials and Methods

The starting materials of this study included Fe₂O₃ (Alfa Aesar Co., <45 μm, 99.5%, Ward Hill, MA, USA), TiO₂ (Alfa Aesar Co., 1–2 μm, 99.5%), Al (Showa Chemical Co., <45 μm, 99.9%, Tokyo, Japan), Fe (Alfa Aesar Co., <45 μm, 99.5%), and amorphous boron (Noah Technologies Corp., <1 μm, 92%, San Antonio, TX, USA). Two combustion systems adopting TiO₂, Fe₂O₃, and Al as the thermite reagents were prepared. Reaction (1) has a variable molar ratio of TiO₂ to Fe₂O₃ and is to produce Fe₃Al–TiB₂–Al₂O₃ composites with different contents of TiB₂. On the other hand, the molar proportion between the two oxide precursors is fixed and equal to unity in Reaction (2) and the resulting composites contain different amounts of Fe₃Al.



where the stoichiometric coefficients, x and y , signify the molar contents of TiB₂ and Fe₃Al formed in Fe₃Al/TiB₂/Al₂O₃ composites based upon Reactions (1) and (2), respectively. Reactant mixtures were formulated with $0.3 \leq x \leq 1.0$ in Reaction (1) and $1.0 \leq y \leq 1.6$ in Reaction (2) to attain stable and self-sustaining combustion.

The reactant powders were well-mixed and compressed into cylindrical samples that were 7 mm in diameter, 12 mm in length, and had a relative density of 60%. The SHS reaction was conducted in a windowed stainless-steel chamber under high purity argon (99.99%) of 0.15 MPa. The combustion wave velocity (V_f) was deduced from the time sequence of recorded images. The combustion temperature (T_c) was measured by a fine-wire (125 μm) Pt/Pt-13%Rh thermocouple attached on the sample surface. Phase constituents of the final product were identified by carrying out phase analyses based on the measured powder X-ray diffraction patterns (Bruker D2) using CuK_α radiation with $\lambda = 1.5406 \text{ \AA}$. The measured XRD patterns were corrected against an external silicon standard. FullProf software (FullProf, Saclay, France) was used for the processing of the data and analyses of the X-ray diffraction patterns. The FullProf program has been mainly developed for the Rietveld analysis of neutron (constant wavelength, time of flight, and nuclear and magnetic scattering) or X-ray powder diffraction data collected at a constant or variable step in scattering angle 2θ [22,23]. The program can be used as

a profile matching (or pattern decomposition using the Le Bail method) tool without knowledge of the structure. Single crystal refinement can also be performed alone or in combination with powder data [23]. The microstructure of the synthesized product was examined under a scanning electron microscope (SEM) (Hitachi, S3000H, Tokyo, Japan) and elemental analysis was performed by energy dispersive spectroscopy (EDS) (Hitachi, S3000H, Tokyo, Japan). The fracture toughness (K_{IC}) of the SHS-derived composite was determined by the indentation method [24]. Details of the experimental methods were previously reported [25].

3. Results and Discussion

3.1. Self-Propagating Combustion Characteristics and Kinetics

Figure 1 presents a typical combustion sequence recorded from the sample of Reaction (1) with $x = 0.5$. It is evident that upon ignition a distinct combustion wave forms and propagates over the starting reactant compact in a self-sustaining manner. Namely, the synthesis reaction proceeds in a form of combustion wave and yields the final product progressively without requiring additional heat. It took about $t = 1.8$ s for the combustion wave to arrive at the bottom of the sample. With an optically superimposed scale on the left-hand side of each image, the flame-front propagation velocity was determined.

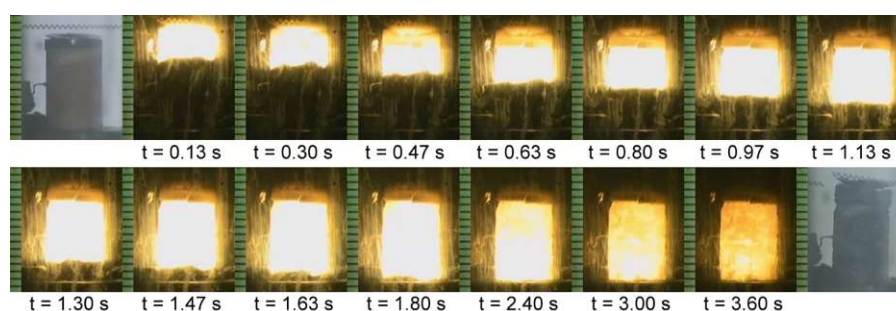


Figure 1. A time sequence of self-propagating combustion images recorded from a powder compact of Reaction (1) with $x = 0.5$.

It is useful to note that the thermite reaction of $\text{Fe}_2\text{O}_3 + 2\text{Al}$ ($\Delta H = -852.3$ kJ and $T_{\text{ad}} = 3622$ K) is much more exothermic than that of $1.5\text{TiO}_2 + 2\text{Al}$ ($\Delta H = -258.7$ kJ and $T_{\text{ad}} = 1799$ K) [26,27]. Therefore, the reaction exothermicity of overall aluminothermic reduction decreases with the increase of x in Reaction (1). It was found in this study that due most likely to insufficient reaction exothermicity, combustion ceased to proceed in Reaction (1) with $x > 1.0$. On the contrary, violent combustion accompanying massive melting of the sample occurred in Reaction (1) with $x < 0.3$, which made both experimental measurement and product recovery difficult.

In Reaction (2), the increase of Fe and Al (i.e., the coefficient y) for the production of more Fe_3Al imposes a dilution effect on combustion, because the formation enthalpy of Fe_3Al ($\Delta H_f = -67$ kJ/mol) is much lower than those of TiB_2 ($\Delta H_f = -315.9$ kJ/mol) and Al_2O_3 ($\Delta H_f = -1675.7$ kJ/mol) [1,27]. The combustibility limit of Reaction (2) was found at $y = 1.6$, beyond which no combustion can be triggered.

For both combustion systems, formation of the $\text{Fe}_3\text{Al-TiB}_2\text{-Al}_2\text{O}_3$ composite proceeds in three consecutive stages [26]. Reduction of Fe_2O_3 by Al to produce Fe and Al_2O_3 is believed to be the initiation step, which is followed by aluminothermic reduction of TiO_2 . Then, the interactions of Fe with Al and Ti with B respectively yield Fe_3Al and TiB_2 .

Variations of the flame-front velocity of Reactions (1) and (2) are shown in Figure 2 with respect to their corresponding stoichiometric coefficients x and y . As revealed in Figure 2, the combustion front velocity of Reaction (1) first increases with x , approaches to a maximum of about 5.88 mm/s at $x = 0.6$, and then decreases with a further increase in x . This is because the influence of the

sample stoichiometry of Reaction (1) on combustion velocity is attributed to two competing factors. With the increase of x , the amount of TiO_2 increases but that of Fe_2O_3 decreases in the starting mixture, thus resulting in a decline in reaction exothermicity of the overall aluminothermic reduction. On the other hand, the content of TiB_2 formed in the product increases as the coefficient x rises and TiB_2 is a highly exothermic phase with $\Delta H_f = -315.9 \text{ kJ/mol}$ [27]. The observation in Figure 2 for Reaction (1) implies that the latter concern governs when the sample stoichiometry varies from $x = 0.3$ to 0.6 , beyond which the former factor becomes dominant. As a result, the flame-front velocity dropped to around 1.02 mm/s at $x = 1.0$.

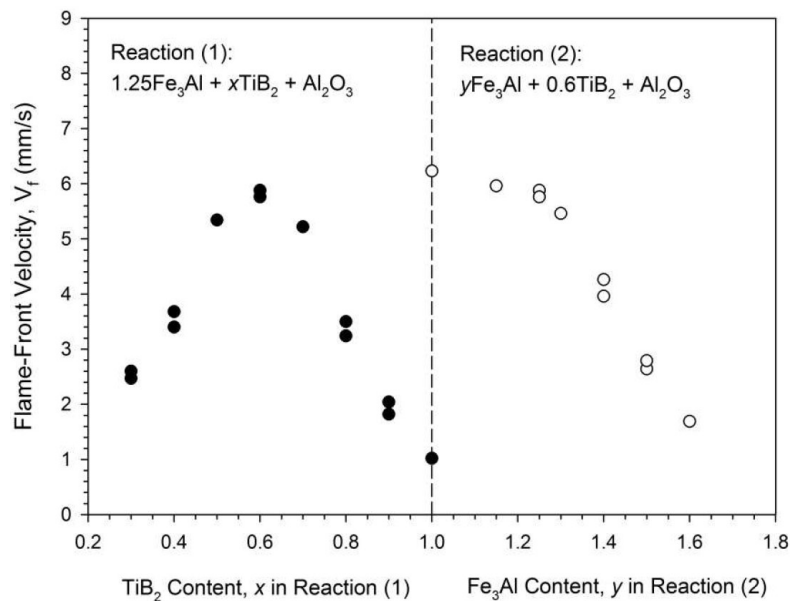


Figure 2. Effects of stoichiometric coefficients (x and y) on flame-front velocities of Reactions (1) and (2) for combustion synthesis of $\text{Fe}_3\text{Al-TiB}_2\text{-Al}_2\text{O}_3$ composites.

Figure 2 also points out that the combustion wave speed of Reaction (2) decreases with increasing y value. The increase of y in Reaction (2) is to enlarge the content of Fe_3Al formed from metallic Fe and Al without varying the composition of thermite reagents and the amount of TiB_2 . As mentioned above, the formation enthalpy of Fe_3Al is relatively low in comparison to that of TiB_2 and the heat released from the reduction of Fe_2O_3 and TiO_2 by Al. Therefore, the increase of y from 1.0 to 1.6 reduced the overall combustion exothermicity of Reaction (2) and led to deceleration of the combustion wave from 6.23 to 1.69 mm/s .

Typical combustion temperature profiles recorded from the powder compacts of Reactions (1) and (2) with different stoichiometries are depicted in Figure 3. The abrupt rise in temperature signifies a rapid arrival of the combustion wave and the peak value corresponds to the combustion front temperature. After the passage of the combustion wave, an appreciable temperature drop is a consequence of heat loss to the surroundings. Profiles #1, #2, and #3 in Figure 3 are associated with Reaction (1) with $x = 0.3$, 0.6 , and 0.8 and their peak temperatures are 1157 , 1514 , and $1277 \text{ }^\circ\text{C}$, respectively. This suggests that the variation of combustion front temperature of Reaction (1) with TiB_2 content is in a manner consistent with that of flame-front velocity. For Reaction (1), the highest combustion front temperature of $1514 \text{ }^\circ\text{C}$ was detected from the sample of $x = 0.6$.

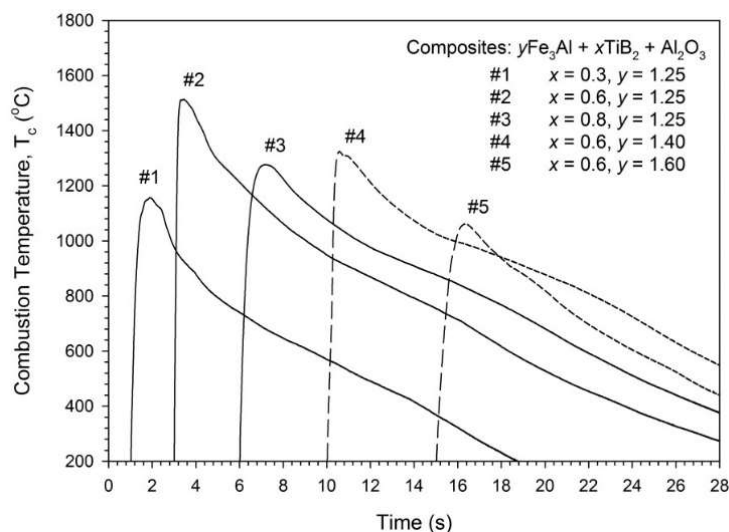


Figure 3. Variations of combustion temperature with TiB_2 and Fe_3Al contents of $\text{Fe}_3\text{Al-TiB}_2\text{-Al}_2\text{O}_3$ composites synthesized by self-propagating high-temperature synthesis (SHS) involving reduction reactions.

Profiles #4 and #5 were measured from Reaction (2) with $y = 1.4$ and 1.6 , respectively. It is evident that the increase of Fe_3Al lowers the reaction temperature, which is in agreement with its effect on combustion wave velocity. For Reaction (2), the lowest combustion front temperature was around $1061\text{ }^\circ\text{C}$ as the sample produced the maximum amount of Fe_3Al (i.e., $y = 1.6$). The highest temperature, reaching up to $1524\text{ }^\circ\text{C}$, was observed in the sample of $y = 1.0$.

The apparent activation energy (E_a) of the solid-state combustion reaction can be deduced by realizing the dependence of flame-front velocity on combustion temperature [28]. Figure 4 depicts a plot correlating $\ln(V_f/T_c)^2$ with $1/T_c$ from both Reactions (1) and (2). According to the slope of a best-fitted straight line for the data, $E_a = 86.8\text{ kJ/mol}$ was determined for in situ formation of $\text{Fe}_3\text{Al-TiB}_2\text{-Al}_2\text{O}_3$ composites from the $\text{Fe}_2\text{O}_3/\text{TiO}_2/\text{Al}/\text{Fe}/\text{B}$ combustion reaction. It is useful to note that the activation energy obtained in the present study is close to that of the $\text{Fe}_2\text{O}_3\text{-Al}$ reaction ($E_a = 83.1\text{ kJ/mol}$) [29]. This implies that aluminothermic reduction of Fe_2O_3 plays an important role in leading and facilitating the reaction sequences of the $\text{Fe}_2\text{O}_3/\text{TiO}_2/\text{Al}/\text{Fe}/\text{B}$ combustion system.

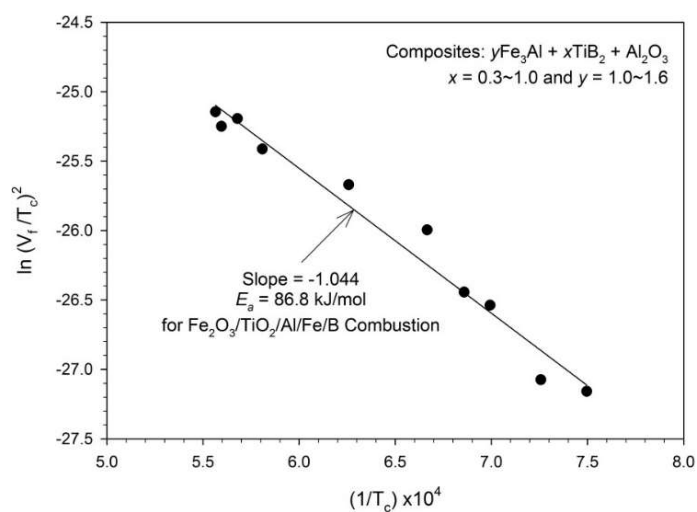


Figure 4. Correlation of combustion front velocity (V_f) with temperature (T_c) for determination of the activation energy (E_a) of $\text{Fe}_2\text{O}_3/\text{TiO}_2/\text{Al}/\text{Fe}/\text{B}$ combustion to produce $\text{Fe}_3\text{Al-TiB}_2\text{-Al}_2\text{O}_3$ composites.

3.2. Phase Constituents and Properties of Synthesized Composites

Figure 5a,b displays the XRD patterns of the final products fabricated from Reaction (1) with $x = 0.5$ and 0.8 , respectively. The as-synthesized products composed of Fe_3Al , TiB_2 , and Al_2O_3 were identified [30]. Figure 5 reveals that with the increase of x the relative intensity of signature peaks of TiB_2 becomes stronger, which is indicative of an increase in TiB_2 formed in the composite.

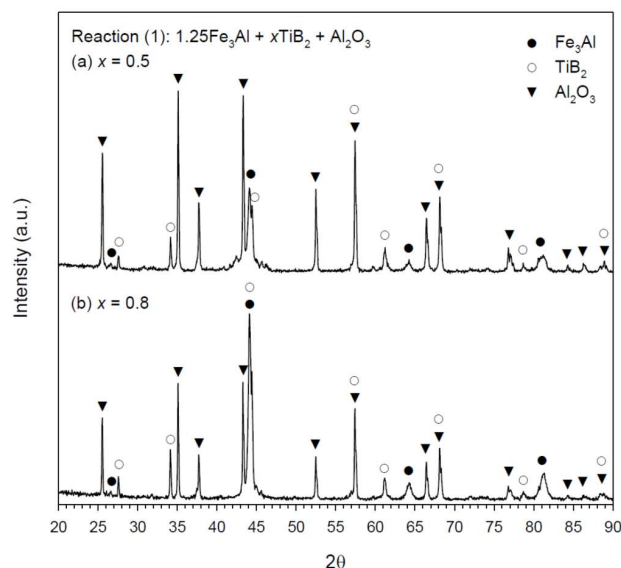


Figure 5. XRD patterns of SHS-derived products from Reaction (1) with (a) $x = 0.5$ and (b) $x = 0.8$.

The phase composition of SHS-derived products from Reaction (2) is presented in Figure 6a,b for $y = 1.0$ and 1.5 , respectively. Complete conversion from the reactants to products of Fe_3Al , TiB_2 , and Al_2O_3 was achieved. The characteristic peaks of Fe_3Al in Figure 6b exhibit much higher intensity than those in Figure 6a. This confirms that more Fe_3Al was produced from the SHS process as Reaction (2) contains additional metallic Fe and Al. In summary, the composition range of the $\text{TiB}_2/\text{Al}_2\text{O}_3$ -added Fe_3Al composites produced in this study can be described by $y\text{Fe}_3\text{Al} + x\text{TiB}_2 + \text{Al}_2\text{O}_3$ with $x = 0.3$ – 1.0 and $y = 1.0$ – 1.6 .

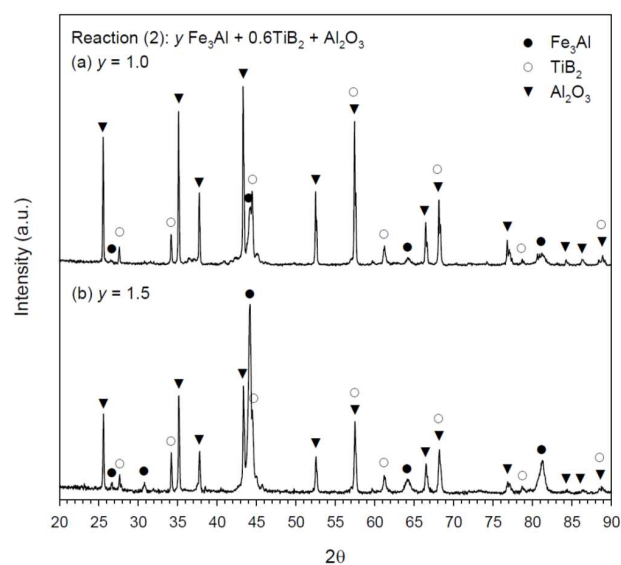


Figure 6. XRD patterns of SHS-derived products from Reaction (2) with (a) $y = 1.0$ and (b) $y = 1.5$.

The relative fraction of constituents was analyzed by the Rietveld refinement for two selected SHS-derived products. The measured lattice parameters (**a** and **c**) of Fe_3Al , TiB_2 , and Al_2O_3 are reported in Table 1. For the composite of $1.25\text{Fe}_3\text{Al} + 0.8\text{TiB}_2 + \text{Al}_2\text{O}_3$ synthesized from Reaction (1), the Rietveld method indicates that the weight percentages are 61.88 wt % of Fe_3Al , 3.72 wt % of TiB_2 , and 24.40 wt % of Al_2O_3 . The relative fractions of Fe_3Al (65.98 wt %), TiB_2 (9.56 wt %), and Al_2O_3 (24.46 wt %) are determined for the composite of $1.5\text{Fe}_3\text{Al} + 0.6\text{TiB}_2 + \text{Al}_2\text{O}_3$ obtained from Reaction (2). It is useful to note that the results of the Rietveld method for the phase composition are in good agreement with those of Reactions (1) and (2).

Table 1. Lattice parameters (**a** and **c**) for the components in two selected composites.

Composites	Components	a (Å)	c (Å)
Reaction (1) with $x = 0.8$	Fe_3Al	5.774	-
	TiB_2	3.027	3.230
	Al_2O_3	4.764	13.002
Reaction (2) with $y = 1.5$	Fe_3Al	5.786	-
	TiB_2	3.024	3.226
	Al_2O_3	4.768	13.005

The typical microstructure of a fracture surface of the SHS-produced $\text{Fe}_3\text{Al-TiB}_2\text{-Al}_2\text{O}_3$ composite is displayed in Figure 7, which presents the product of Reaction (2) with $y = 1.6$. The microstructure exhibits the agglomeration of micro-sized grains. The agglomerates have a dense and contiguous morphology. For those gray agglomerates shown in Figure 7, the EDS analysis indicates their atomic ratio to be $\text{Fe}:\text{Al} = 75.43:24.57$, which matches well with that of Fe_3Al . It is believed that most of the TiB_2 grains are embedded in the agglomerates. The other distinct morphology is characterized by bright alumina grains, whose atomic proportion determined by the EDS spectrum is $\text{Al}:\text{O} = 37.34:62.66$.

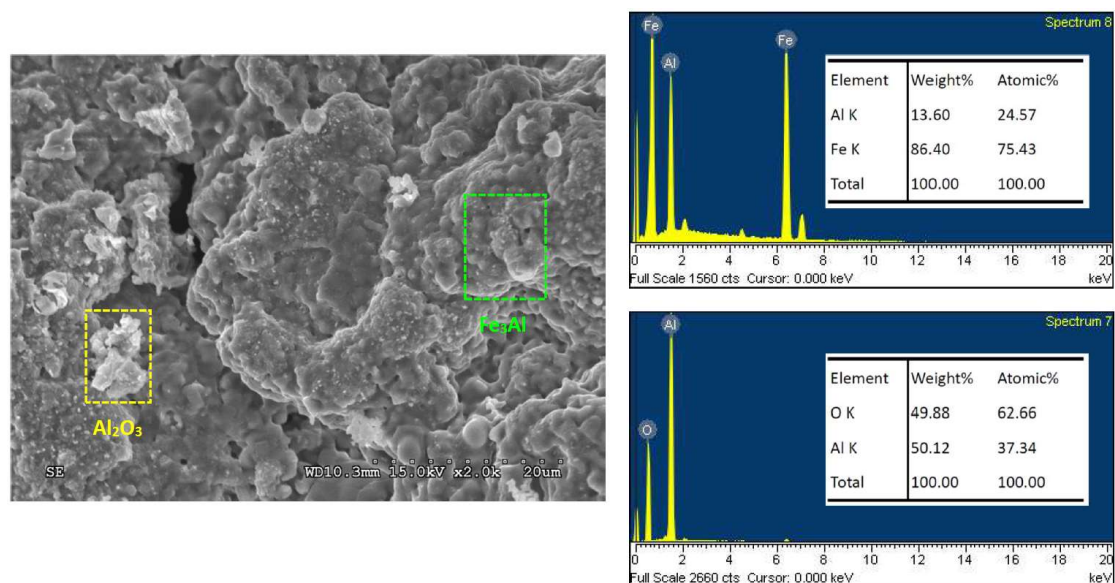


Figure 7. SEM micrograph and EDS spectra of the $\text{Fe}_3\text{Al-TiB}_2\text{-Al}_2\text{O}_3$ composite synthesized from Reaction (2) with $y = 1.6$.

The hardness of the $\text{TiB}_2/\text{Al}_2\text{O}_3$ -added Fe_3Al composites synthesized from Reaction (1) is in the range from 11.2 to 19.6 GPa, which increases with increasing TiB_2 content from $x = 0.3$ to 1.0. Figure 8 shows that as the content of TiB_2 increases, the fracture toughness of the $\text{TiB}_2/\text{Al}_2\text{O}_3$ -reinforced Fe_3Al

composite increases from 5.32 to 7.92 MPa·m^{1/2}. This proves the strengthening effect of the ceramic phases on Fe₃Al.

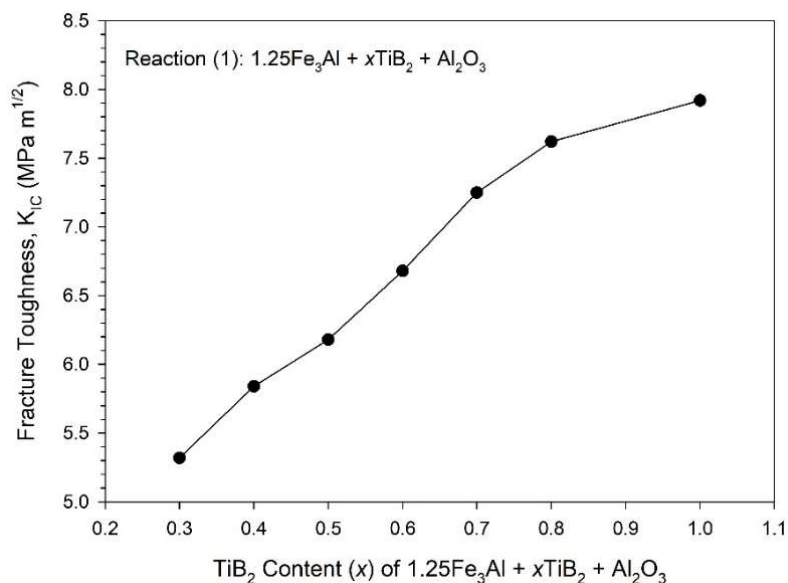


Figure 8. Effect of TiB₂ content on the fracture toughness of 1.25Fe₃Al + xTiB₂ + Al₂O₃ composites synthesized by SHS of Reaction (1).

4. Conclusions

The SHS process involving aluminothermic reduction of oxide precursors was conducted to prepare Fe₃Al–TiB₂–Al₂O₃ composites with a broad range of phase compositions. The starting materials included elemental Fe, amorphous boron, and thermite reagents made up of Fe₂O₃, TiO₂, and Al. Aluminothermic reduction of Fe₂O₃ played an important role in thermally and chemically activating the synthesis reaction in a self-sustaining combustion mode. Experimental results showed that for the production of a higher content of TiB₂ in the composites of 1.25Fe₃Al + xTiB₂ + Al₂O₃ with x = 0.3–1.0, there existed a maximum combustion wave velocity of 5.88 mm/s and a highest reaction front temperature of 1514 °C at x = 0.6. This was caused by the fact that the reaction exothermicity of the thermite mixture decreased but the formation enthalpy of TiB₂ increased. On the other hand, for the increase of Fe₃Al in the product of yFe₃Al + 0.6TiB₂ + Al₂O₃ with y = 1.0–1.6, the additional Fe and Al reduced the overall reaction exothermicity and decelerated the combustion wave. Based upon the dependence of flame-front velocity on combustion temperature, the activation energy (E_a) of 86.8 kJ/mol was determined for the Fe₂O₃/TiO₂/Al/Fe/B combustion system to produce Fe₃Al–TiB₂–Al₂O₃ composites.

The XRD analysis of the as-synthesized products indicated that complete conversion from the reactants to Fe₃Al–TiB₂–Al₂O₃ composites was achieved. Two SHS systems capable of varying the molar contents of TiB₂ and Fe₃Al in an effective manner were confirmed. Moreover, it was found that the increase of TiB₂ from x = 0.3 to 1.0 in the 1.25Fe₃Al + xTiB₂ + Al₂O₃ composites contributed to an increase in fracture toughness from 5.32 to 7.92 MPa·m^{1/2}.

Acknowledgments: This research was sponsored by the Ministry of Science and Technology of Taiwan under the grant of MOST 105-2221-E-035-039-MY2. The authors are grateful for the Precision Instrument Support Center of Feng Chia University in providing materials analysis facilities.

Author Contributions: Chun-Liang Yeh conceived and designed the experiments, analyzed the experimental data, supervised the work, and wrote the paper. Chih-Yao Ke performed the SHS experiments and materials analysis.

Conflicts of Interest: The authors declare no conflict of interest.

References

1. Deevi, S.C.; Sikka, V.K. Nickel and iron aluminides: An overview on properties, processing, and applications. *Intermetallics* **1996**, *4*, 357–375. [[CrossRef](#)]
2. Stoloff, N.S. Iron aluminides: Present status and future prospects. *Mater. Sci. Eng. A* **1998**, *258*, 1–14. [[CrossRef](#)]
3. Joslin, D.L.; Easton, D.S.; Liu, C.T.; Babu, S.S.; David, S.A. Processing of Fe₃Al and FeAl alloys by reaction synthesis. *Intermetallics* **1995**, *3*, 467–481. [[CrossRef](#)]
4. Schneibel, J.H.; Carmichael, C.A.; Specht, E.D.; Subramanian, R. Liquid-phase sintered iron aluminide-ceramic composites. *Intermetallics* **1997**, *5*, 61–67. [[CrossRef](#)]
5. Itoi, T.; Mineta, S.; Kimura, H.; Yoshimi, K.; Hirohashi, M. Fabrication and wear properties of Fe₃Al-based composites. *Intermetallics* **2010**, *18*, 2169–2177. [[CrossRef](#)]
6. Amiriyan, M.; Blais, C.; Savoie, S.; Schulz, R.; Cariépy, M.; Alamdari, H.D. Mechanical behavior and sliding wear studies on iron aluminide coatings reinforced with titanium carbides. *Metals* **2017**, *7*, 177. [[CrossRef](#)]
7. Amiriyan, M.; Blais, C.; Savoie, S.; Schulz, R.; Cariépy, M.; Alamdari, H. Trio-mechanical properties of HVOF deposited Fe₃Al coatings reinforced with TiB₂ particles for wear-resistance applications. *Materials* **2016**, *9*, 117. [[CrossRef](#)] [[PubMed](#)]
8. Peng, L.M.; Li, H.; Wang, J.H.; Gong, M. High strength and high fracture toughness ceramic-iron aluminide (Fe₃Al) composites. *Mater. Lett.* **2006**, *60*, 883–887. [[CrossRef](#)]
9. Li, J.; Kwong, F.; Shi, R.; Ng, D.H.L.; Yin, Y. Microstructure and properties of in situ nanometric Al₂O₃ reinforced α -Fe(Al)-Fe₃Al-based composites. *Mater. Sci. Eng. A* **2009**, *526*, 50–55. [[CrossRef](#)]
10. Khodaei, M.; Enayati, M.H.; Karimzadeh, F. The structure and mechanical properties of Fe₃Al-30 vol. % Al₂O₃ nanoparticles. *J. Alloys Compd.* **2009**, *488*, 134–137. [[CrossRef](#)]
11. Subramanian, R.; MaKamey, C.G.; Buck, L.R.; Schneibel, J.H. Synthesis of iron aluminide-Al₂O₃ composites by in-situ displacement reactions. *Mater. Sci. Eng. A* **1997**, *239–240*, 640–646. [[CrossRef](#)]
12. Sharifitabar, M.; Vahdati Khaki, J.; Haddad Sabzevar, M. Formation mechanism of TiC-Al₂O₃-Fe₃Al composites during self-propagating high-temperature synthesis of TiO₂-Al-C-Fe system. *Ceram. Int.* **2016**, *42*, 12361–12370. [[CrossRef](#)]
13. Liu, Y.; Cai, X.; Sun, Z.; Jiao, X.; Akhtar, F.; Wang, J.; Feng, P. A novel fabrication strategy for highly porous FeAl/Al₂O₃ composite by thermal explosion in vacuum. *Vacuum* **2018**, *149*, 225–230. [[CrossRef](#)]
14. Merzhanov, A.G. Combustion and explosion processes in physical chemistry and technology of inorganic materials. *Russ. Chem. Rev.* **2003**, *72*, 289–310. [[CrossRef](#)]
15. Liu, G.; Li, J.; Chen, K. Combustion synthesis of refractory and hard materials: A review. *Int. J. Refract. Met. Hard Mater.* **2013**, *39*, 90–102. [[CrossRef](#)]
16. Levashov, E.A.; Mukasyan, A.S.; Rogachev, A.S.; Shtansky, D.V. Self-propagating high-temperature synthesis of advanced materials and coatings. *Int. Mater. Rev.* **2017**, *62*, 203–239. [[CrossRef](#)]
17. Yeh, C.L.; Peng, J.A. Combustion synthesis of MoSi₂-Al₂O₃ composites from thermite-based reagents. *Metals* **2016**, *6*, 235. [[CrossRef](#)]
18. Yeh, C.L.; Chong, M.H. Effects of B₄C and BN additions on formation of NbB₂-Al₂O₃ composites from reduction-based Combustion synthesis. *Ceram. Int.* **2017**, *43*, 7560–7564. [[CrossRef](#)]
19. Yeh, C.L.; Sung, W.Y. Combustion synthesis of Ni₃Al intermetallic compound in self-propagating mode. *J. Alloys Compd.* **2004**, *384*, 181–191. [[CrossRef](#)]
20. Yeh, C.L.; Su, S.H. In situ formation of TiAl-TiB₂ composite by SHS. *J. Alloys Compd.* **2006**, *407*, 150–156. [[CrossRef](#)]
21. Yeh, C.L.; Ke, C.Y.; Chen, Y.C. In situ formation of TiB₂/TiC and TiB₂/TiN reinforced NiAl by self-propagating combustion synthesis. *Vacuum* **2018**, *151*, 185–188. [[CrossRef](#)]
22. Young, R.A.; Wiles, D.B. Profile shape functions in Rietveld refinements. *J. Appl. Cryst.* **1982**, *15*, 430–438. [[CrossRef](#)]
23. Rodriguez-Carvajal, J. Recent developments of the program FULLPROF. *Newsl. Comm. Powder Diffr.* **2001**, *26*, 12–19.
24. Evans, A.G.; Charles, E.A. Fracture toughness determinations by indentation. *J. Am. Ceram. Soc.* **1976**, *59*, 371–372. [[CrossRef](#)]

25. Yeh, C.L.; Lin, J.Z. Combustion synthesis of Cr-Al and Cr-Si intermetallics with Al₂O₃ additions from Cr₂O₃-Al and Cr₂O₃-Al-Si reaction systems. *Intermetallics* **2013**, *33*, 126–133. [[CrossRef](#)]
26. Wang, L.L.; Munir, Z.A.; Maximov, Y.M. Thermite reactions: Their utilization in the synthesis and processing of materials. *J. Mater. Sci.* **1993**, *28*, 3693–3708. [[CrossRef](#)]
27. Binnewies, M.; Milke, E. *Thermochemical Data of Elements and Compounds*; Wiley-VCH Verlag GmbH: Weinheim, Germany, 2002.
28. Bertolino, N.; Anselmi-Tamburini, U.; Maglia, F.; Spinolo, G.; Munir, Z.A. Combustion synthesis of Zr-Si intermetallic compounds. *J. Alloys Compd.* **1999**, *288*, 238–248. [[CrossRef](#)]
29. Rafiei, M.; Enayati, M.H.; Karimzadeh, F. Kinetic analysis of thermite reaction in Al-Ti-Fe₂O₃ system to produce (Fe,Ti)₃Al-Al₂O₃ nanocomposite. *Powder Technol.* **2014**, *253*, 553–560. [[CrossRef](#)]
30. Mighell, A.D.; Karen, V.L. NIST crystallographic databases for research and analysis. *J. Res. Natl. Inst. Stand. Technol.* **1996**, *101*, 273–280. [[CrossRef](#)] [[PubMed](#)]



© 2018 by the authors. Licensee MDPI, Basel, Switzerland. This article is an open access article distributed under the terms and conditions of the Creative Commons Attribution (CC BY) license (<http://creativecommons.org/licenses/by/4.0/>).